Large area, patterned growth of 2D MoS2 and lateral MoS2–WS2 heterostructures for nano- and opto-electronic applications

Nanotechnology

PAPER • OPEN ACCESS

Large area, patterned growth of 2D MoS_2 and lateral MoS_2–WS_2 heterostructures for nano- and opto-electronic applications

To cite this article: Akhil Sharma *et al* 2020 *Nanotechnology* **31** 255603

OPEN ACCESS
IOP Publishing
Nanotechnology

Nanotechnology **31** (2020) 255603 (12pp)
https://doi.org/10.1088/1361-6528/ab7593

Large area, patterned growth of 2D MoS_2 and lateral MoS_2–WS_2 heterostructures for nano- and opto-electronic applications

Akhil Sharma[1], Reyhaneh Mahlouji[1], Longfei Wu[2], Marcel A Verheijen[1,3], Vincent Vandalon[1], Shashank Balasubramanyam[1], Jan P Hofmann[2], W M M (Erwin) Kessels[1] and Ageeth A Bol[1]

[1] Department of Applied Physics, Eindhoven University of Technology, PO Box 513, 5600 MB Eindhoven, The Netherlands
[2] Laboratory of Inorganic Materials and Catalysis, Department Chemical Engineering and Chemistry, Eindhoven University of Technology, PO Box 513, 5600 MB Eindhoven, The Netherlands
[3] Eurofins Materials Science, High Tech Campus 11, 5656 AE Eindhoven, The Netherlands

E-mail: a.a.bol@tue.nl

Received 5 January 2020
Accepted for publication 12 February 2020
Published 7 April 2020

Abstract

The patterned growth of transition metal dichalcogenides (TMDs) and their lateral heterostructures is paramount for the fabrication of application-oriented electronics and optoelectronics devices. However, the large scale patterned growth of TMDs remains challenging. Here, we demonstrate the synthesis of patterned polycrystalline 2D MoS_2 thin films on device ready SiO_2/Si substrates, eliminating any etching and transfer steps using a combination of plasma enhanced atomic layer deposition (PEALD) and thermal sulfurization. As an inherent advantage of ALD, precise thickness control ranging from a monolayer to few-layered MoS_2 has been achieved. Furthermore, uniform films with exceptional conformality over 3D structures are obtained. Finally, the approach has been leveraged to obtain in-plane lateral heterostructures of 2D MoS_2 and WS_2 thin films over a large area which opens up an avenue for their direct integration in future nano- and opto-electronic device applications.

Supplementary material for this article is available online

Keywords: PEALD, MoS_2, patterned growth, lateral heterostructures, large area

(Some figures may appear in colour only in the online journal)

Introduction

Layered two-dimensional (2D) transition metal dichalcogenides (TMDs) offer an exciting platform for myriad optoelectronic applications owing to their ultra-thin bodies and extraordinary broad spectrum of electrical, mechanical, and optical properties [1–3]. The integration of atomically thin TMDs also gives rise to extremely interesting new physical phenomena, such as interband tunneling, optospintronics etc [4, 5]. Amongst the family of TMDs, MoS_2 is one of the most studied materials due to its high earth abundance, stability in ambient and amenability to get aligned in heterostructure based architectures [6]. A massive effort has been put into studying various properties of mechanically-exfoliated MoS_2 on the lab scale [7–11], however, the lack of homogeneous spatial distribution and low yield hinders the scalable production of 2D layers with the exfoliation method. Therefore, there is a quest for developing scalable growth techniques capable of producing high quality films with precise thickness control over large areas. To address this, bottom-up synthesis methods have been employed to produce 2D TMDs over

large areas. Amongst these methods, chemical vapor deposition (CVD) is the most widely accepted technique [12–15], and is capable of producing high quality material with large grain size, yet it is difficult to achieve accurate control over thickness and uniformity. Moreover, the direct, large-area production of high quality TMDs on device-ready substrates with CVD remains a challenge, as the highest quality CVD material is often obtained on sapphire substrates. To be able to deposit high quality TMDs on device-ready substrates is one of the foremost prerequisites for realizing high performance electronic devices. Generally, the CVD grown TMDs are transferred to a relevant substrate using a polymer-based transfer technique which often results in polymer contamination causing interface degradation. Subsequently, the device fabrication proceeds with post patterning of transferred material involving usage of a masking layer (usually photo/electron beam resists), followed by an etching step which might further exacerbate the magnitude of degradation. One of the possible solutions to evade this issue is the patterned growth of TMDs directly on device-ready substrates which will not only reduce the device fabrication steps (i.e. typical reactive ion etching of TMDs), but also minimize the degree of possible polymer contamination inferred by the transfer process.

The patterned growth of TMDs is an important aspect for realizing advanced electronic device architectures as manifested by a recent widespread attention in the literature [16–21]. The majority of work available in the literature is based on either surface functionalization or use of pre-patterned seeded areas. The first methodology relies often on the selective blocking of TMD growth by using pristine graphene or hydrophobic polymers [16–18]. For instance, Bersch *et al* have demonstrated a method based on surface modification by using a hydrophobic polymer functional layer (PFL) to preclude TMD nucleation and growth resulting in selective area growth of MoS_2 [18]. Other approaches to achieve patterned growth of MoS_2 is the pre-patterning of parent MoO_3 material using lithography or shadow mask, and subsequent sulfurization which can produce contamination free, high quality MoS_2 films with pristine surfaces [19, 22, 23]. Han *et al* have demonstrated the synthesis of MoS_2 monolayer islands at pre-defined locations by sulfurization of lithographically patterned bead shaped MoO_3 *seeds* prepared by physical vapor deposition [19]. This approach has been referred to as *seeded growth* of MoS_2 monolayers. However, small regions of multilayer material and poor pattern fidelity (irregularity in shape of flakes) were observed which is an undesirable attribute for practical applications. Young *et al* have used SiN stencils to produce resist free, templated Mo films which are subsequently sulfurized to yield a MoS_2 monolayer on controlled locations with sub-micron feature sizes on sapphire substrates [20]. Although, high quality and layer-controlled MoS_2 films are produced by this technique, the preparatory need of the focused ion beam to pattern SiN membranes increases the overall complexity of the process and makes it challenging for industrial implementation. Additionally, the pattern scaling remains limited due to the lateral dimensions of the SiN membrane. An interesting approach by Song *et al* based on pre-patterning of an Au–Mo alloy as parent material and subsequent thermal sulfurization enabled the easy transfer of patterned few-layered MoS_2 to arbitrary substrates [21]. However, clustering of metal source and co-existence of unreacted Au–Mo alloy after sulfurization might deteriorate the opto-electronic properties. Given this background, it is clear that the controllable synthesis of TMDs with high crystallinity and of desired thickness, at specific locations is imperative for their successful fabrication and subsequent device integration. It is worth mentioning that the precise thickness control down to atomic scale during synthesis of TMDs is crucial as the properties of TMDs are directly governed by number of 2D layers.

Another application-oriented merit of patterned growth for 2D TMDs is the possibility to realize lateral heterostructures. These heterostructures have gained significant attention in recent years due to their potential applications for the next generation nano-electronic device schemes and more specifically as the main building blocks for tunneling field effect transistors (TFETs) [24–26]. Many groups have addressed the formation of lateral heterostructures using methods like CVD based edge epitaxy and lithography patterning [27–34]. These heterostructures are composed of a central TMD crystal surrounded by a dissimilar TMD crystal on their periphery. A wide variety of applications ranging from p–n junctions, localized photoluminescence enhancement, photovoltaics and photodetector etc has been demonstrated using these heterostructures [28–30, 33]. Although very high quality TMD heterostructures (i.e. seamless, sharp and coherent) have been obtained by using the above mentioned synthesis methods, the lack of precise control over their thickness, uniformity and geometry calls for additional alternative scalable methods.

Here, we demonstrate an atomic layer deposition (ALD) based approach to achieve transfer-free patterned growth of 2D MoS_2 at predefined locations with atomic thickness control on a wafer scale in combination with high pattern fidelity. The key distinguishing feature of our approach is the use of ALD, which, inherently yields atomic-scale thickness control combined with excellent uniformity and conformality; a combination of properties not reported so far for the synthesis of lateral heterostructures. Moreover, the combination of top-down nanoscale patterning with a bottom-up chemical method eliminates the need of film transfer and any reactive ion etching step to achieve patterned growth of polycrystalline 2D MoS_2. The top-down nanoscale patterning of MoO_x (deposited by PEALD) has been attained by employing electron beam lithography (EBL). The patterned MoO_x thin film serves as parent material for the controlled growth of mono- to- few layered polycrystalline MoS_2 at predefined locations on SiO_2/Si substrates. The use of PEALD allows for low temperature processing (50 °C), which is indispensable for the primary steps in processing on top of a resist, enabling high pattern fidelity and eliminating the need of any etching step. In the second phase, the patterned MoO_x is sulfurized at high temperature (900 °C) using H_2S + Ar gas. The work-flow proposed and demonstrated in this work yields thickness-controlled, large-area polycrystalline MoS_2 films

directly on device-ready substrates without the need for a transfer process. The excellent conformality over 3D structures inherent to ALD will be demonstrated in a separate experiment on a 3D nano-trench structure. In literature, it has been shown that the integration of 2D TMDs on unconventional substrates with tailored geometry/functionality can offer vast opportunities for a variety of applications including gas sensor, photo detection and imaging, optoelectronics etc [35–37]. Furthermore, our PEALD based approach provides a route towards formation of seamless in-plane lateral heterostructures of 2D MoS_2 and WS_2 layers in a controlled way on technologically relevant SiO_2/Si substrates. We thus show a proof-of-principle by forming atomically thin 2D lateral heterostructures grown on predefined locations and with desirable shape over a large area, demonstrating the feasibility of our approach towards integration of heterostructures for nano- and opto-electronic applications.

The first three sections of this paper discuss the PEALD enabled patterned growth of MoS_2 and the detailed characterization of the obtained layers, including the uniformity and conformality. The final section of paper demonstrates the formation of lateral heterostructures of MoS_2 and WS_2 thin layers and the related characterization. Our work presents a supplementary path to the range of approaches adopted in literature for obtaining lateral heterostructures targeting towards future generation devices and integrated circuits.

Experimental methods

Thin film growth

The MoO_x (WO_x) thin films were deposited at 50 °C in an Oxford Instruments FlexAL^{TM} ALD reactor on 4″ Si wafers with a thermally grown 90 or 450 nm thick SiO_2 layer on top. The Mo (W) precursor employed was $[(NtBu)_2(NMe_2)_2Mo]$ ($[(NtBu)_2(NMe_2)_2W]$), (98%, Strem Chemicals) and was contained in a stainless-steel canister which was heated to 50 °C. At this temperature, the vapor pressure of the precursor is reported to be 0.13 Torr [38]. The delivery lines were kept at 90 °C to avoid condensation of the precursor while the reactor walls were heated to 50 °C. For the precursor delivery to the deposition chamber, a 100 sccm Ar (>99.999% purity) bubbling flow was employed. An intermediate Ar purge step with 100 sccm of Ar flow was applied after each precursor and plasma exposure steps. As the co-reactant, an O_2 plasma was employed as generated in an inductively coupled plasma (ICP) source using 50 sccm O_2 gas. The plasma power was 100 W with a reactor pressure of 6.6 mTorr during the plasma step. The ALD recipe was established with the first half cycle consisting of precursor dosing for 6 s followed by 6 s purge. The second half cycle consisted of 8 s of plasma exposure followed by 6 s purge. The detailed characterization of the PEALD process at 50 °C for MoO_x can be found in the previous work from our group [39].

The film thickness evolution during deposition was monitored by *in situ* spectroscopy ellipsometry (J A Woollam M2000F, 1.25–5 eV). For MoO_x films, a general oscillator model in the SE modeling was used to analyze the thickness evolution during PEALD process. A combination of Tauc-Lorentz and Gaussian oscillators were used to account for the interband absorption and absorption below the band gap at low photon energy (∼1 eV) respectively.

Thermal sulfurization, patterning and lateral heterostructures

MoO_x and WO_x thin films were sulfurized in a tube furnace at 900 °C under atmospheric pressure. A combination of H_2S + Ar gas (10% H_2S) was used as sulfurization gas. The recipe employed for thermal sulfurization is shown in figure S1 is available online at stacks.iop.org/NANO/31/255603/mmedia (supporting information). The patterned MoO_x films were obtained by using conventional EBL. Poly (methyl methacrylate) (PMMA) type A4 was used as e-beam resist. For lift-off of PMMA layer, acetone (⩾99.5%) was used as the solvent. A Cauchy dispersion model was used to extract the thickness of the PMMA from the SE data. Finally, the fabrication scheme for lateral heterostructures is provided in the figure S7 (supporting information).

Characterization

Raman spectroscopy (RS) and photoluminescence (PL) spectroscopy measurements were performed with a Renishaw InVia Raman microscope equipped with a 514 nm laser, integrated switchable gratings with 600 or 1800 lines/mm, and a CCD detector. For each Raman scan, 5 accumulations with acquisition time of 10 s were taken using a laser power of <0.2 mW focused on a ∼1 μm region. Atomic force microscopy (AFM) was also employed to study the surface topology of the as-deposited films. The images were acquired at room temperature on a Veeco dimension 3100 system operated in tapping mode using Al coated Si tip (PointProbe Plus-NCHR) having a radius <7 nm. Images were processed in Gwyddion software and RMS roughness was obtained statistically from a scan area of 500 × 500 nm^2. The patterned structures before and after sulfurization process were characterized with a Zeiss Axio Imager 2 Optical microscope. To determine the elemental composition, x-ray photoelectron spectroscopy (XPS) was performed using a Thermo Scientific K-alpha spectrometer (Thermo Fisher Scientific, Waltham, MA) equipped with a monochromatic Al Kα x-ray radiation source ($h\nu$ = 1486.6 eV). For the XPS point and line scan analyses, a 400 μm and 50 μm diameter spots were used respectively. The photoelectrons were collected at a take-off angle of 60°. The samples were neutralized during the XPS analysis using an electron flood gun in order to correct for differential or non-uniform charging. All peaks in the XPS survey scans are referenced to the binding energy of the C1s peak of adventitious carbon (284.8 eV) for charge correction and quantification of the survey scans have been performed using Avantage software. The selectivity of MoS_2 line bars was determined by energy dispersive x-ray spectroscopy (EDX) with an EDAX UMSII EDX spectrometer integrated in a scanning electron microscope (FEI Nova 600i DualBeam system). The film microstructure was studied by Transmission

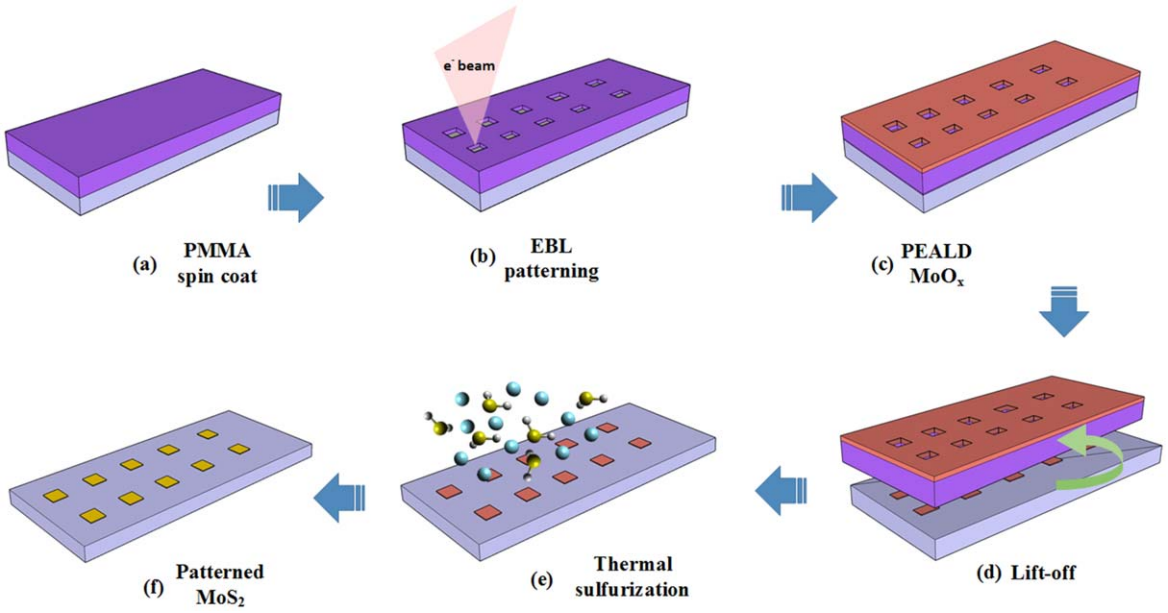

Figure 1. (a)–(f) The scheme shows the process flow for the ALD enabled patterned growth of large area MoS_2.

electron microscopy (TEM) analysis using a probe corrected JEOL ARM 200 F operated at 80 kV, using both the bright field TEM mode and the high angle annular dark field (HAADF) scanning TEM mode. Atomic resolution imaging of the poly-crystalline MoS_2 film was performed in HAADF-STEM mode using a camera length of 20 cm; at this camera length, some diffraction contrast is present, enhancing the visibility of the crystal dimensions. For the top planar view images, MoO_x films were grown on SiN_x TEM windows, coated with ~5 nm ALD SiO_2, which were subsequently thermally sulfurized at 900 °C. Selected area electron diffraction (SAED) patterns were acquired from a 1.3 μm diameter area on each sample. The conformality of the MoS_2 ALD process was determined on substrate coupons with high aspect ratio (HAR) nanostructures. These HAR nanostructures were created by etching PECVD grown SiO_2 on a Si wafer. The SiO_2 nanostructures were then coated with a SiN_x layer deposited by high-temperature CVD, onto which a SiO_2 thin film was deposited using ALD. Prior to focused ion beam (FIB) sample preparation, the MoS_2 sample was coated with a layer of spin-on epoxy to fill the remaining gaps in the trenches and to protect the film from curtaining damage during the subsequent lift-out FIB sample preparation.

Results and discussion

ALD enabled patterned growth of MoS_2

A simplified scheme of the process flow which we used to obtain the patterned MoS_2 films is given in figures 1(a)–(f). As shown, firstly, the SiO_2/Si substrates are spin-coated with Poly (methyl methacrylate) (PMMA) and subsequently patterned using EBL (figures 1(a) and (b)). Thereafter, MoO_x is deposited using low temperature PEALD (50 °C) which covers the patterned regions and the surrounding PMMA as depicted in figure 1(c). Next, the resist and unwanted MoO_x are removed using standard lift-off techniques resulting in isolated patterns of MoO_x (figure 1(d)). These MoO_x patterns are thermally sulfurized at 900 °C (figure 1(e)), resulting in patterned MoS_2 squares (10 × 10 μm^2) (see figure 1(f)). It is to be noted that any residual PMMA remaining after the lift-off process is removed in the subsequent high temperature thermal sulfurization process which ensures pristine MoS_2 films.

It is important to realize here that the low growth temperature (50 °C) during PEALD (figure 1(c)) is the key to attain high fidelity patterned MoS_2 films. The conventional polymers (such as PMMA) used for lithography have a low glass transition temperature, low plasma etch resistance and therefore might suffer from reflowing issues and plasma damage during a standard ALD process at higher temperature. However, it has been demonstrated earlier that the use of low temperatures during PEALD enables metal oxide deposition on polymer substrates including PMMA without any reflowing issues [40]. In our case, since we also use low temperature (50 °C) during PEALD, we were able to deposit MoO_x on PMMA without damage/reflowing of PMMA. In order to investigate this, we monitored the change in thickness of PMMA during MoO_x deposition using *in situ* spectroscopic ellipsometry (figure S2 in supporting information). It was observed that the PMMA thickness was slightly reduced only during few initial PEALD cycles and thereafter MoO_x could be deposited without any damage to the PMMA layer underneath.

The assessment of patternability attained for MoS_2 (figure 1(f)) was performed using Raman spectroscopy. Figure 2(a) shows the Raman spectra for the patterned region with and without MoS_2. It is clearly evident that the characteristic Raman signal is visible only for regions with MoS_2 which confirms the patternability achieved using the process flow as described above. Furthermore, notably the MoS_2 squares retain the pre-defined geometry and therefore yield high fidelity of the targeted patterns which is difficult to

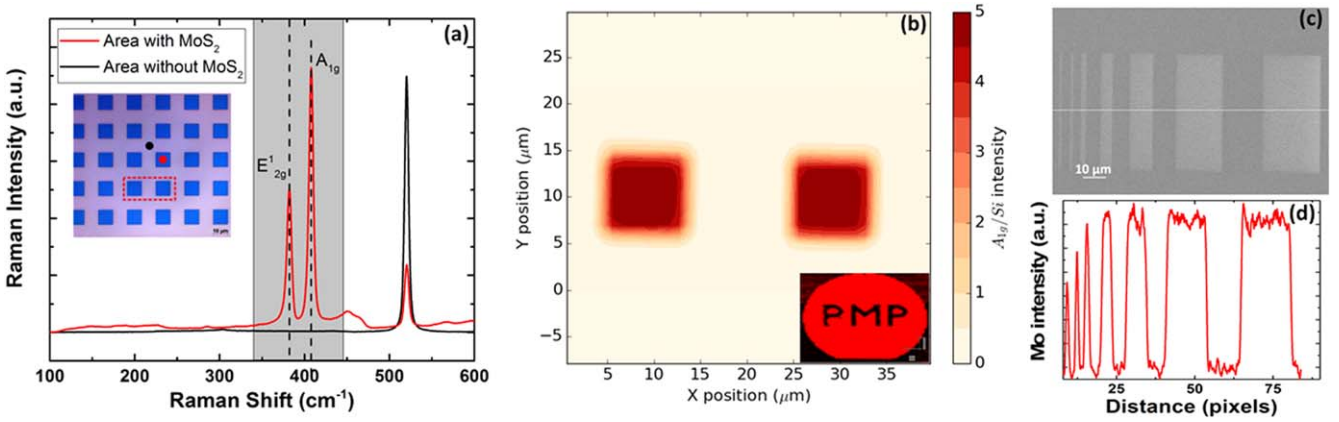

Figure 2. (a) Raman spectra of regions with and without patterned MoS_2. These regions are indicated by the red and blue dots on the optical microscopy image of patterned MoS_2 respectively, as shown in the inset. The region with characteristic vibrational Raman modes is highlighted by the gray band. (b) Raman mapping image of the region consisting of two patterned MoS_2 squares highlighted by the dashed square in the inset of (a). Note that the intensity drop-off observable at the edge regions can be attributed to the large spot size ($\sim$1 μm) of the laser beam. The inset shows the PL mapping image for a pattern containing the acronym of our research group (PMP). The region with letters (black) represents the SiO_2 substrate while the red color corresponds to the MoS_2 monolayer. (c) SEM image showing the patterned MoS_2 line bars with width ranging from 0.8 to 25 μm. (d) The EDX line profile (overlaid) clearly displays the Mo signal appearing from the patterned regions.

achieve with some methods based on the 'seeded growth' as described previously (see figure S3 in supporting information). In order to assess the homogeneity of the film on the patterned areas, we performed a mapping of the spatial distribution of the out-of-plane Raman vibrational mode (A_{1g}) using a diffraction-limited beam spot and a step size of $\sim$200 nm. The out-of-plane (A_{1g}) Raman mode is one of the characteristic vibrational modes observed for MoS_2 (discussed below). Figure 2(b) shows the area map for fitted peak intensity of the A_{1g} vibrational mode across the area shown in the optical micrograph (inset of figure 2(a)). A homogeneous Raman signal is obtained over the entirety of the patterned area and no signal is observed outside the pattern, displaying an excellent selectivity of the MoS_2 films while retaining the pre-defined geometry. Further, in order to demonstrate the versatility of our process, we developed a pattern containing the acronym 'PMP' of our research group 'Plasma and Material Processing' surrounded by a monolayer MoS_2. The corresponding PL map is shown in the inset of figure 2(b). The Raman frequency difference (Δ) of 20.6 cm^{-1} (not shown) registers the presence of a monolayer on the patterned area (as discussed later).

Additionally, a SEM-EDX line scan was performed on sub-μm features (line bars) containing MoS_2 film (figures 2(c) and (d)), which clearly shows the presence of Mo species only in the patterned areas and confirms the nanoscale patternability of our process. These results demonstrate the viability of our ALD based process as an effective route to achieve patternable large area synthesis of mono-to-few layered 2D MoS_2 thin films.

Patterned polycrystalline 2D MoS_2 films

The parent patterned MoO_x films with different thicknesses were obtained by varying the number of ALD cycles (10–60) during the PEALD process. This subsequently resulted into systematic controllability over thickness of resultant MoS_2 films. The thicknesses of the initial patterned MoO_x (before sulfurization) films as assessed by *in situ* spectroscopic ellipsometry during the PEALD process are given in the supporting information (table S1 in supporting information). To confirm the precise controllability over number of layers in MoS_2 films, AFM was used to measure the height of patterned MoS_2 films. Figures 3(a) and (b) shows the AFM images for the monolayer (10 ALD cycles) and few layered (60 cycles) samples respectively.

The measured heights were $\sim$1 nm and 4.5 nm respectively. The larger measured height of $\sim$1 nm than expected for a monolayer (0.65 nm) might be attributed to the effect of distinct tip-sample and tip-substrate interactions as reported in the literature [41]. Concurrently, the 4.5 nm (60 cycles) thick sample indicates 7–8 layers, which is in accordance with the Raman analysis ($\Delta = 25.8\ cm^{-1}$) (as discussed below) and therefore confirms the precise thickness control achievable with ALD. The topography of the films was also studied using AFM. The corresponding images are shown in figure S4 (supporting information) which reveals smooth polycrystalline films with a roughness in the range of 0.2–0.3 nm which is comparable to the roughness of the underlying Si substrate.

The thickness and crystalline quality of patterned MoS_2 films with varied thickness were characterized by Raman spectroscopy. Figure 3(c) shows the progression of the Raman vibrational modes with increasing thickness of the MoS_2 film on SiO_2/Si substrates. The two characteristic vibrational modes (i.e. A_{1g} and E^1_{2g}) are clearly visible for all the samples investigated. The frequency difference (Δ) between the two vibrational modes generally increases with increasing number of layers present in the MoS_2 film and thus is used as an indicator to determine the number of layers [42].

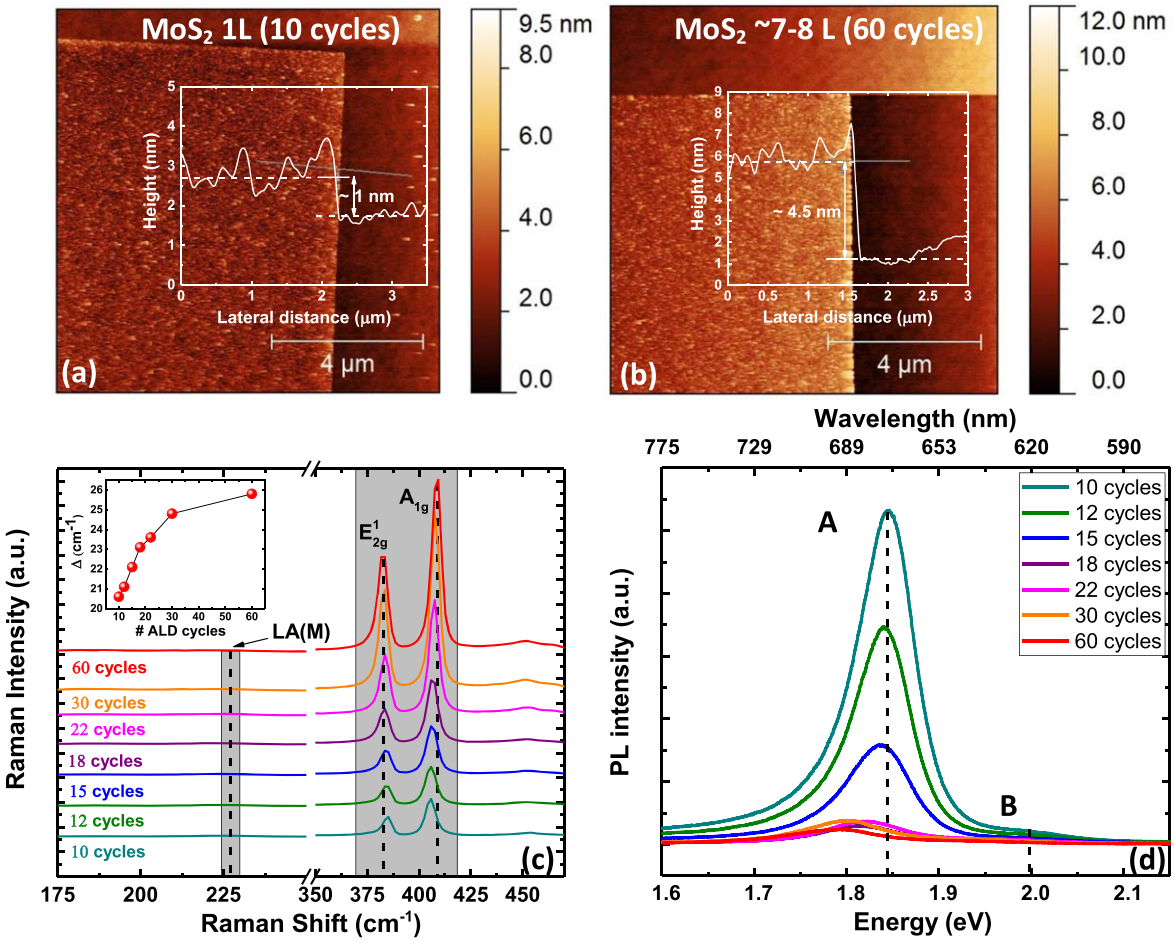

Figure 3. (a) and (b) AFM images of the polycrystalline mono and few-layered MoS_2 films. The insets in both images show the measured height at the edge of the patterns of 1 and 4.5 nm for the mono and few-layered films respectively. (c) Raman spectra showing the progression of two vibrational modes with increasing thickness of MoS_2 film. The regions with two predominant vibrational modes and LA (M) mode at low Raman frequency region (~227 cm^{-1}) are highlighted in gray. The inset shows the increasing frequency difference (Δ) as a function of increasing film thickness (increasing number of ALD cycles for parent MoO_x film). (d) Photoluminescence (PL) spectra showing strong emission for a monolayer (10 cycles) associated with the A and B exciton at 1.85 eV and 2.0 eV, respectively. The intensity thereafter reduces as the thickness of MoS_2 film increases with the increasing number of ALD cycles for parent MoO_x films.

In our case, 'Δ' increases monotonically (20.6–26.2 cm^{-1}) with increasing number of MoO_x ALD cycles (from 10 to 60 cycles) which indicates the formation of monolayer to thick film (~7 to 8 layers). Thus, by controlling the number of MoO_x ALD cycles, a systematic control over the thickness of the final MoS_2 films is attained. It is noteworthy that the value of 'Δ' increases in a continuous manner with increasing number of ALD cycles, i.e. a value of 21.1 cm^{-1} is obtained (for 12 cycles) amidst formation of a monolayer (20.6 cm^{-1}) to bilayer (22.3 cm^{-1}) after 10 and 15 cycles, respectively. This is a consequence of the typical sub-monolayer film growth per ALD cycle.

Furthermore, it has been reported that the structural defects in the MoS_2 film can be quantified by assessing a low frequency peak at ~227 cm^{-1} in the Raman spectrum [43]. This peak is assigned to the longitudinal acoustic phonons at the M point of the Brillouin zone and denoted as LA(M) [43, 44]. The Raman spectra in figure 3(c) do not show the LA(M) mode in all the samples investigated, pointing towards a good quality of the films obtained after thermal sulfurization. Moreover, the full width half maximum (FWHM) values of the in-plane vibrational peak (E^1_{2g}) for all samples remain in the range of 4.6–5.0 cm^{-1}, which is comparable with the typical CVD grown polycrystalline material [45–47], reaffirming the good quality of our samples. The photoluminescence (PL) results are in line with the Raman analysis and the corresponding spectra are shown in figure 3(d). A strong signal at ~674 nm and a weak shoulder at ~623 nm are observed for a monolayer (10 ALD cycles) material, which corresponds to the A and B excitonic peaks associated with the direct band gap transitions [48]. The PL intensity subsequently becomes weaker with increasing number of layers in the MoS_2 films owing to a transition to thick MoS_2 with an indirect band gap [9].

The microstructure of patterned MoS_2 films was characterized by high resolution transmission electron microscopy (HRTEM) analysis. The cross-sectional HAADF-STEM image for few-layered (~8 to 9 layers) MoS_2 film (70 cycles) shown in figures 4(a) and (b) reveals the ordered in-plane oriented layers grown on SiO_2/Si substrate corroborating the good quality of the MoS_2 film. The STEM image shown in

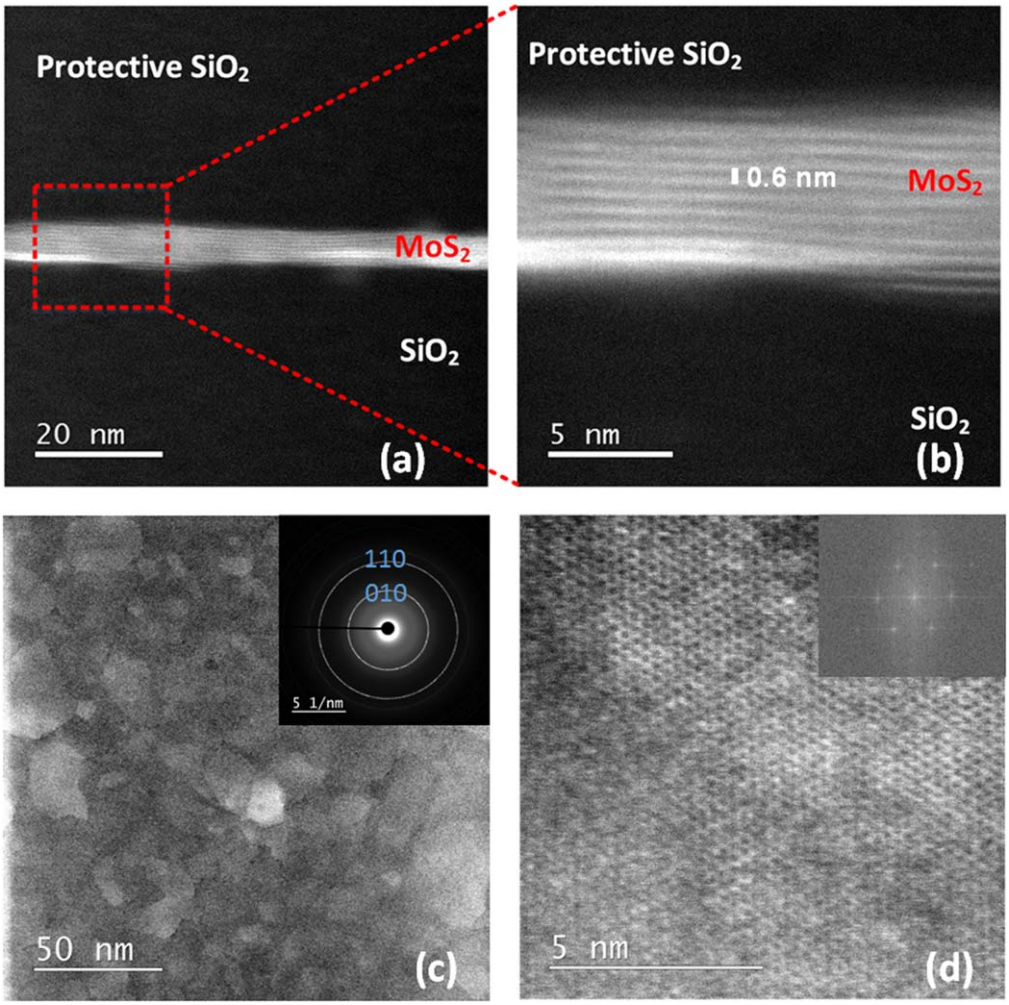

Figure 4. (a) Cross-sectional HAADF-STEM image showing a few layered (7–8 layered) MoS_2 film on SiO_2/Si substrate. (b) The magnified image clearly reveals the individual layers stacked on each other with interlayer distance of ∼0.6 nm (as highlighted). (c) Top view STEM image showing the uniform coverage of the polycrystalline MoS_2 film. The inset shows a selective area electron diffraction pattern from the same sample which confirms the polycrystalline, textured nature of the film. (d) High resolution STEM image showing the hexagonal atomic arrangement and the corresponding FFT pattern (inset) clearly displaying the sixfold symmetry of MoS_2.

figure 4(c) allows to gain additional microstructural insights. The uniform surface coverage of polycrystalline MoS_2 film with grain size in the few to 50 nm range is clearly displayed. The polycrystalline nature of MoS_2 film is further confirmed by SAED (figure 4(c)) which shows the closed rings corresponding to randomly oriented nanodomains. The presence of the 110 and 010 rings and the absence of a 002 ring reflects the ⟨002⟩ texture of the film.

Further, the HAADF-STEM image in figure 4(d) reveals the hexagonal arrangement of atoms, again displaying the in-plane orientation of the MoS_2 layers of the 2-H phase. An additional analysis of this image is presented in figure S5 (supporting information). The chemical composition of the films before and after sulfurization was examined by x-ray photoelectron spectroscopy (XPS). It is noteworthy to mention that the MoO_x films deposited at 50 °C before sulfurization are sub-stoichiometric in nature. This is evident from a clearly observable shoulder on the Mo3d peak corresponding to oxygen vacancies in agreement with earlier reports [38].

After sulfurization, the oxidation state of the Mo in MoS_2 films was found to be predominantly Mo^{4+} based on the binding energy position for Mo3d peaks. The stoichiometry of the MoS_2 after sulfurization ranged between 2.0 and 2.2 for all samples which confirms the good quality of the films. A more comprehensive discussion of the XPS results, high-resolution spectra of Mo3d, S2p, O1s peaks with detailed peak assignments can be found in figure S6 (supporting information).

Large area and conformal 2D MoS_2 films

As mentioned earlier, ALD is capable of producing films with wafer scale uniformity and high conformality on intricate structures. We therefore assessed both these attributes for our resultant MoS_2 films as well. In order to confirm the wafer scale uniformity of our process, a Raman line scan was performed over 9 points (1 cm apart) on a 10 cm wafer strip. Figure 5(a) shows the Raman vibrational modes corresponding to measured points for a sample with 7–8 layers

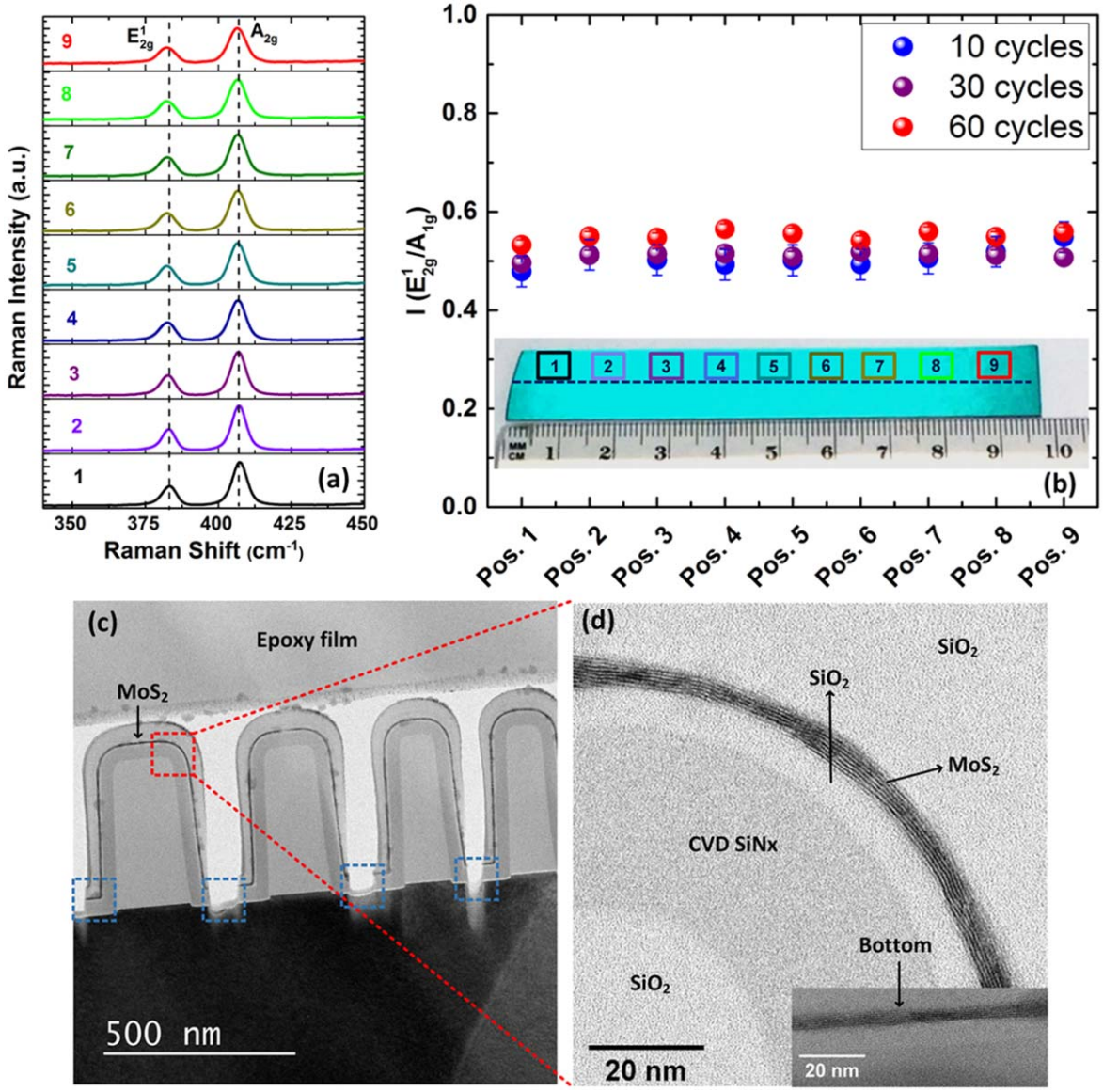

Figure 5. (a) The plot shows the homogenous Raman spectral features throughout the 9 different scanned areas on the wafer strip (~10 cm) which is shown as inset of (b). The resultant MoS_2 film is 7–8 layers obtained in this case with 60 cycles of ALD processed for the parent MoO_x film. (b) A consistent intensity ratio between two Raman vibrational modes across the measured points for samples with varying number of ALD cycles confirms the uniform nature of the film over large area. The wafer strip (~10 cm in length) with different measurement points is shown in the inset. (c) The cross-sectional TEM image shows the conformal MoS_2 coating on high-aspect ratio nanostructures. Note: the highlighted areas (—) were damaged during FIB preparation of the sample due to insufficient filling of voids by the protective epoxy film (i.e. part of the TEM sample preparation) as shown. (d) The magnified image of a curved section from one of the trench structures clearly reveals the conformal coverage of layered MoS_2 on the planar surface and side wall and thus registering the conformal nature of our PEALD based approach. The inset shows the bottom planar part of the same trench structure where the similar conformal coverage of MoS_2 is obtained.

(60 ALD cycles). The consistent Raman peaks along the scanned region reveal the homogenous crystalline nature of the MoS_2 film. In addition, figure 5(b) shows the integrated intensity ratio between two peaks ($I(E^1_{2g})/I(A_{1g})$) for samples with varying MoS_2 thickness over the 9 measured points. This integrated ratio increases slightly with increasing number of layers which is attributed to the optical field enhancement phenomenon affecting both vibrational modes equally with increasing number of layers [49]. The intensity ratios for the investigated samples with different thicknesses (i.e. 10 cycles, 30 cycles, 60 cycles) over the measured points remain spatially homogeneous which demonstrates both the high quality and large area uniformity of MoS_2 films.

The conformality of the films was investigated using high-aspect ratio (HAR) nano-sized trench structures with varying aspect ratios (depth = 394 nm and width = 44–650 nm) as shown in figure 5(c). It is evident that the 7–8 layered thick MoS_2 uniformly coats the trench structures. A magnified image of a trench structure (figure 5(d)) shows an excellent conformality on both the side walls and planar areas of the HAR structure. A markedly high conformality of 88% (side walls with respect to planar area) was evaluated for a trench structure

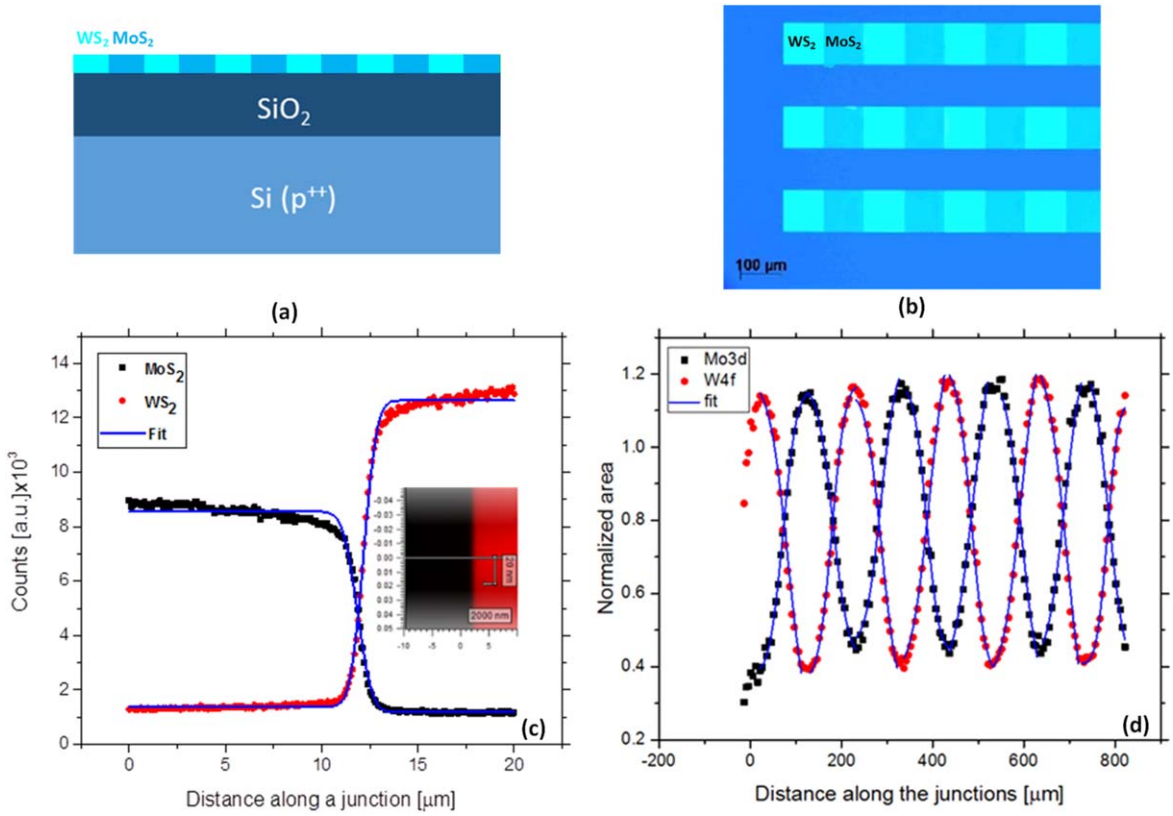

Figure 6. (a) Schematic cross-section of the as-fabricated structures (b) Top-view optical microscope image of the final lateral WS_2/MoS_2 hetero-structures with dimensions of $100 \times 100\ \mu m^2$ (scale bar is 100 μm) (c) Raman line scan of a WS_2/MoS_2 heterojunction. The black and red dots represent the intensity of the A_{1g} vibrational mode for MoS_2 and WS_2 respectively, while the solid line is the numerical fitting. The inset shows the region of interest probed by Raman line scan. (d) The XPS line scan across several lateral features (length of 700 μm) showing the intensity of Mo3d and W4f signals and solid line representing the numerical fit.

with an aspect ratio (AR) of 12 (AR = depth/width). Recently, Martella *et al* have demonstrated a high degree of conformality for MoS_2 growth on nano-trench patterns using a similar approach as ours by combining ALD and CVD [35]. It has been shown that MoS_2 bending on curvatures of trenches dramatically affects the electron phonon coupling as characterized by resonant Raman scattering and thus paves the path to manipulation of opto-electronic properties of TMDs. Likewise, some next generation 3D applications based on 2D materials might get benefit from this particular aspect attainable by ALD [36]. Based on the above results, it can be concluded that ALD enables a way to synthesize layer controlled 2D MoS_2 films in combination with high uniformity and excellent conformality over 3D structures.

Lateral growth of 2D heterostructures

The integration of atomically thin TMDs to create lateral heterostructures is an extremely interesting area of research for numerous future applications [4, 5]. However, despite the high technological relevance, there is still a lack of feasible methods to obtain sharp and seamless lateral stitching of heterostructures. In this context, we have leveraged our technique based on EBL and low temperature PEALD (as discussed above) to realize lateral heterostructures of MoS_2 and WS_2 thin films. To this purpose, we have implemented a two-step process flow identical to that as shown in figure 4 by combining the patterns of MoS_2 and WS_2 in a lateral fashion. The detailed description along with the simplified schematic of the process used are given in supporting information (figure S7). Figures 6(a) and (b) show the schematic cross-section and optical microscopy image of the fabricated lateral hetero-structure patterns, respectively. The interface abruptness between WS_2 and MoS_2 was assessed by performing a Raman line scan encompassing 20 μm across the interface with a step size of 0.1 μm. The corresponding spatial distribution of intensity for out-of-plane (A_{1g}) Raman vibrational modes for both WS_2 and MoS_2 is plotted in figure 6(c) which shows a smooth transition at the interface of heterojunction. This smooth transition is mainly attributed to the limited incident beam spot size ($\sim$1 μm) which was further supported by modeling the shape of the line profiles using a normalized Gaussian distribution with Heaviside step function. The full width half maximum (FWHM) of the numerical fitting for both MoS_2 and WS_2 line profile was on average 570.1 ± 30 nm similar to the expected diffraction limited radius of the spot size used in the Raman experiment, clearly ascertaining that the interface is sharper than 1 μm. In addition, figure 6(d) shows the XPS line scan which was performed along 700 μm over the patterns (as shown in figure 6(b)) with a step size of 5 μm. The observed periodic profiles for Mo3d and W4f scans are in complete accordance

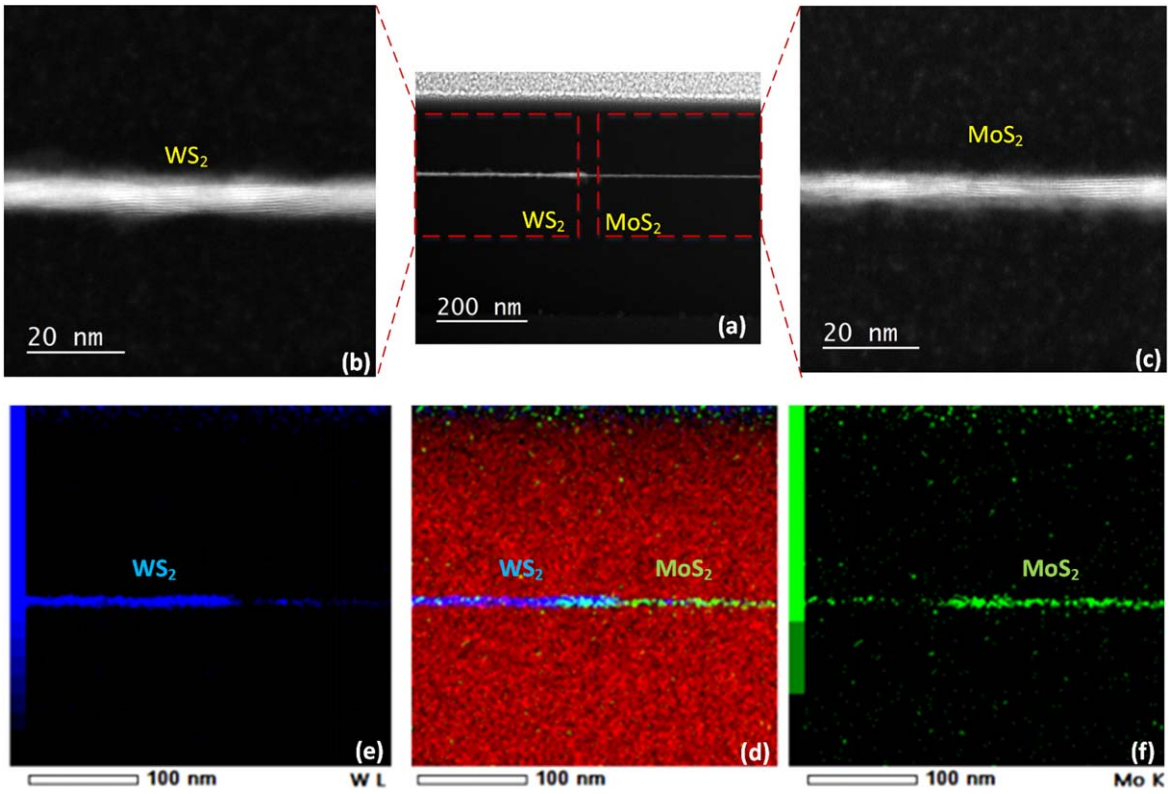

Figure 7. (a) Low magnification cross-sectional HR-STEM characterization of WS_2/MoS_2 junction. Magnified cross-sectional HR-STEM images of (b) WS_2 and (c) MoS_2 regions. Low magnification STEM-EDX elemental maps of (d) as-fabricated hetero-structure (e) WS_2 region and (f) MoS_2 region.

with the Raman line scan results and reconfirm the formation of a seamless interface. Moreover, a homogeneous line profile obtained for S2p (not shown here) for both WS_2 and MoS_2 regions clearly indicates towards the formation of stoichiometric thin films.

A cross sectional HAADF-STEM image of the junction in low magnification mode is shown in figure 7(a) in which the two well-defined regions of WS_2 and MoS_2 can be distinguished. The individual regions of WS_2 and MoS_2 in higher magnification mode are shown in figures 7(b) and (c) respectively. The images clearly indicate the layered structure of MoS_2 and WS_2 processed by the two-step synthesis technique (as mentioned earlier). In addition to HAADF-STEM images, STEM-EDX elemental mapping of the hetero-structure is provided in figure 7(d). Despite the partial overlap (~30 nm) of W and Mo, figures 7(e) and (f) respectively reveal the predominance of WS_2 on the left side and MoS_2 on the right side of the heterojunction further confirming the precise pattern fidelity by means of EBL. The partial overlap observed at the heterojunction is most likely due to misalignment of the adjacent patterns during EBL process used and further process optimization should mitigate this.

Conclusion

In this paper, we have demonstrated a PEALD based approach coupled with EBL which can enable patternable synthesis of 2D MoS_2 over a large area without the need of a transfer process and etching. The approach has also been leveraged to obtain in-plane lateral heterostructures of 2D WS_2 and MoS_2 thin films which paves a path towards a broad range of future nano- and opto-electronic applications. In addition, the large area uniformity and a high conformality of the in-plane oriented layered MoS_2 over intricate 3D structures have been demonstrated owing to the innate characteristics of ALD. Raman and PL spectroscopy have revealed the precise thickness control and polycrystalline nature of patterned MoS_2 films with high fidelity attained by our PEALD based process. Overall, a powerful technique with high controllability and scalability has been developed which could be readily extended to form other 2D materials based hetero-structures for ultrathin electronics.

Acknowledgments

This work has been funded by the European Research Council (Grant Agreement No. 648787-ALDof2DTMDs). Further, this work has also been supported by NWO and Technology Foundation STW through the VIDI program on 'Novel bottom-up nanofabrication techniques for future carbon-nanoelectronics'. Solliance and the Dutch province of Noord Brabant are acknowledged for funding the TEM facility. The authors gratefully acknowledge J van Gerwen, C A A van Helvoirt, J J L M Meulendijks, C O van Bommel and

J J A Zeebregts for their technical assistance. Dr Beatriz Barcones is acknowledged for carrying out the FIB sample preparation for TEM analysis. The authors are also thankful to LAM Research for providing substrates with HAR trench nanostructures.

ORCID iDs

Akhil Sharma https://orcid.org/0000-0003-1837-3262
Marcel A Verheijen https://orcid.org/0000-0002-8749-7755
W M M (Erwin) Kessels https://orcid.org/0000-0002-7630-8226
Ageeth A Bol https://orcid.org/0000-0002-1259-6265

References

[1] Huang X, Zeng Z and Zhang H 2013 Metal dichalcogenide nanosheets: preparation, properties and applications *Chem. Soc. Rev.* **42** 1934–46
[2] Zhang H 2015 Ultrathin two-dimensional nanomaterials *ACS Nano* **9** 9451–69
[3] Kang K, Xie S, Huang L, Han Y, Huang P Y, Mak K F, Kim C-J, Muller D and Park J 2015 High-mobility three-atom-thick semiconducting films with wafer-scale homogeneity *Nature* **520** 656–60
[4] Nourbakhsh A, Zubair A, Dresselhaus M S and Palacios T 2016 Transport properties of a MoS_2/WSe_2 heterojunction transistor and its potential for application *Nano Lett.* **16** 1359–66
[5] Gmitra M and Fabian J 2015 Graphene on transition-metal dichalcogenides: a platform for proximity spin–orbit physics and optospintronics *Phys. Rev.* B **92** 155403 –1
[6] Ganatra R and Zhang Q 2014 Few-layer MoS_2: a promising layered semiconductor *ACS Nano* **8** 4074–99
[7] Novoselov K S, Jiang D, Schedin F, Booth T J, Khotkevich V V, Morozov S V and Geim A K 2005 Two-dimensional atomic crystals *Proc. Natl Acad. Sci. USA* **102** 10451–3
[8] Chhowalla M, Shin H S, Eda G, Li L-J, Loh K P and Zhang H 2013 The chemistry of two-dimensional layered transition metal dichalcogenide nanosheets *Nat. Chem.* **5** 263–75
[9] Eda G, Yamaguchi H, Voiry D, Fujita T, Chen M and Chhowalla M 2011 Photoluminescence from chemically exfoliated MoS_2 *Nano Lett.* **11** 5111–6
[10] Coleman J N *et al* 2011 Two-dimensional nanosheets produced by liquid exfoliation of layered *Mater. Sci.* **331** 568–71
[11] Yao Y, Lin Z, Li Z, Song X, Moon K-S and Wong C-P 2012 Large-scale production of two-dimensional nanosheets *J. Mater. Chem.* **22** 13494–9
[12] Najmaei S, Liu Z, Zhou W, Zou X, Shi G, Lei S, Yakobson B I, Idrobo J-C, Ajayan P M and Lou J 2013 Vapour phase growth and grain boundary structure of molybdenum disulphide atomic layers *Nat. Mater.* **12** 754–9
[13] van der Zande A M, Huang P Y, Chenet D A, Berkelbach T C, You Y, Lee G-H, Heinz T F, Reichman D R, Muller D A and Hone J C 2013 Grains and grain boundaries in highly crystalline monolayer molybdenum disulphide *Nat. Mater.* **12** 554–61
[14] Chen J *et al* 2016 Chemical vapor deposition of high-quality large-sized MoS_2 crystals on silicon dioxide substrates *Adv. Sci.* **3** 1500033
[15] Ling X, Lee Y-H, Lin Y, Fang W, Yu L, Dresselhaus M S and Kong J 2014 Role of the seeding promoter in MoS_2 growth by chemical vapor deposition *Nano Lett.* **14** 464–72
[16] Xi L *et al* 2016 Parallel stitching of 2D materials *Adv. Mater.* **28** 2322–9
[17] Chen X, Park Y J, Das T, Jang H, Lee J-B and Ahn J-H 2016 Lithography-free plasma-induced patterned growth of MoS_2 and its heterojunction with graphene *Nanoscale* **8** 15181–8
[18] Brian M B, Sarah M E, Yu-Chuan L, Kehao Z, Ganesh R B, Aleksander F P, Michael L III and Joshua A R 2017 Selective-area growth and controlled substrate coupling of transition metal dichalcogenides *2D Mater.* **4** 025083
[19] Han G H *et al* 2015 Seeded growth of highly crystalline molybdenum disulphide monolayers at controlled locations *Nat. Commun.* **6** 6128
[20] Young J R *et al* 2017 Uniform large-area growth of nanotemplated high-quality monolayer MoS_2 *Appl. Phys. Lett.* **110** 263103
[21] Song I, Park C, Hong M, Baik J, Shin H-J and Choi H C 2014 Patternable large-scale molybdenium disulfide atomic layers grown by gold-assisted chemical vapor deposition *Angew. Chem. Int. Ed.* **53** 1266–9
[22] Woods J M, Jung Y, Xie Y, Liu W, Liu Y, Wang H and Cha J J 2016 One-step synthesis of MoS_2/WS_2 layered heterostructures and catalytic activity of defective transition metal dichalcogenide films *ACS Nano* **10** 2004–9
[23] Xue Y *et al* 2016 Scalable production of a few-layer MoS_2/WS_2 vertical heterojunction array and its application for photodetectors *ACS Nano* **10** 573–80
[24] Li M O, Yan R, Jena D and Xing H G 2016 In two-dimensional heterojunction interlayer tunnel FET (Thin-TFET): From theory to applications *2016 IEEE Int. Electron Devices Meeting (IEDM) (3–7 December 2016pp 2.1–4*
[25] Roy T, Tosun M, Cao X, Fang H, Lien D-H, Zhao P, Chen Y-Z, Chueh Y-L, Guo J and Javey A 2015 Dual-gated MoS_2/WSe_2 van der waals tunnel diodes and transistors *ACS Nano* **9** 2071–9
[26] Ilatikhameneh H, Tan Y, Novakovic B, Klimeck G, Rahman R and Appenzeller J 2015 Tunnel field-effect transistors in 2D transition metal dichalcogenide materials *IEEE J. Exploratory Solid-State Comput. Devices Circuits* **1** 12–8
[27] Taghinejad H, Eftekhar A A and Adibi A 2019 Lateral and vertical heterostructures in two-dimensional transition-metal dichalcogenides [Invited] *Opt. Mater. Express* **9** 1590–607
[28] Li M-Y *et al* 2015 Epitaxial growth of a monolayer WSe_2-MoS_2 lateral p-n junction with an atomically sharp interface *Science* **349** 524–8
[29] Gong Y *et al* 2014 Vertical and in-plane heterostructures from WS_2/MoS_2 monolayers *Nat. Mater.* **13** 1135
[30] Gong Y *et al* 2015 Two-step growth of two-dimensional $WSe_2/MoSe_2$ heterostructures *Nano Lett.* **15** 6135–41
[31] Sahoo P K, Memaran S, Xin Y, Balicas L and Gutiérrez H R 2018 One-pot growth of two-dimensional lateral heterostructures via sequential edge-epitaxy *Nature* **553** 63
[32] Zhang Z, Chen P, Duan X, Zang K, Luo J and Duan X 2017 Robust epitaxial growth of two-dimensional heterostructures, multiheterostructures, and superlattices *Science* **357** 788–92
[33] Sahoo P K *et al* 2019 Bilayer lateral heterostructures of transition-metal dichalcogenides and their optoelectronic response *ACS Nano* **13** 12372–84
[34] Duan X *et al* 2014 Lateral epitaxial growth of two-dimensional layered semiconductor heterojunctions *Nat. Nanotechnol.* **9** 1024
[35] Martella C, Ortolani L, Cianci E, Lamperti A, Morandi V and Molle A 2019 Large-area patterning of substrate-conformal MoS_2 nano-trenches *Nano Res.* **12** 1851–4
[36] Sungwoo J, Joon K S, Hyeong-Jun K, Hyung J D, Soo-Yeon C and Hee-Tae J 2017 Highly periodic metal dichalcogenide nanostructures with complex shapes, high resolution, and high aspect ratios *Adv. Funct. Mater.* **27** 1703842

[37] Lee W *et al* 2018 Two-dimensional materials in functional three-dimensional architectures with applications in photodetection and imaging *Nat. Commun.* **9** 1417
[38] Vos M F J, Macco B, Thissen N F W, Bol A A and Kessels W M M 2016 Atomic layer deposition of molybdenum oxide from $(NtBu)_2(NMe_2)_2Mo$ and O_2 plasma *J. Vac. Sci. Technol.* A **34** 01A103
[39] Macco B, Vos M F J, Thissen N F W, Bol A A and Kessels W M M 2015 Low-temperature atomic layer deposition of MoO_x for silicon heterojunction solar cells *Phys. Status Solidi* **9** 393–6
[40] Kääriäinen T O, Lehti S, Kääriäinen M L and Cameron D C 2011 Surface modification of polymers by plasma-assisted atomic layer deposition *Surf. Coat. Technol.* **205** S475–9
[41] Song J-G *et al* 2013 Layer-controlled, wafer-scale, and conformal synthesis of tungsten disulfide nanosheets using atomic layer deposition *ACS Nano* **7** 11333–40
[42] Lee C, Yan H, Brus L E, Heinz T F, Hone J and Ryu S 2010 Anomalous lattice vibrations of single- and few-layer MoS_2 *ACS Nano* **4** 2695–700
[43] Mignuzzi S, Pollard A J, Bonini N, Brennan B, Gilmore I S, Pimenta M A, Richards D and Roy D 2015 Effect of disorder on Raman scattering of single-layer MoS_2 *Phys. Rev.* B **91** 195411
[44] Elisha M, Andy G, Jonathan M, Mike C and Ravi S S 2017 A Raman metrology approach to quality control of 2D MoS_2 film fabrication *J. Phys. D: Appl. Phys.* **50** 184005
[45] Yi-Hsien L *et al* 2012 Synthesis of large-area MoS_2 atomic layers with chemical vapor deposition *Adv. Mater.* **24** 2320–5
[46] Yu Y, Li C, Liu Y, Su L, Zhang Y and Cao L 2013 Controlled scalable synthesis of uniform, high-quality monolayer and few-layer MoS_2 films *Sci. Rep.* **3** 1866
[47] Zhang J *et al* 2014 Scalable growth of high-quality polycrystalline MoS_2 monolayers on SiO_2 with tunable grain sizes *ACS Nano* **8** 6024–30
[48] Splendiani A, Sun L, Zhang Y, Li T, Kim J, Chim C-Y, Galli G and Wang F 2010 Emerging photoluminescence in monolayer MoS_2 *Nano Lett.* **10** 1271–5
[49] Bera A and Sood A K 2014 Insights into vibrational and electronic properties of MoS_2 using raman, photoluminescence, and transport studies *MoS_2: Materials, Physics, and Devices* ed Z M Wang (Cham: Springer International Publishing) pp 155–215